ChemistryOpen

Review
doi.org/10.1002/open.202200091

Chemistry
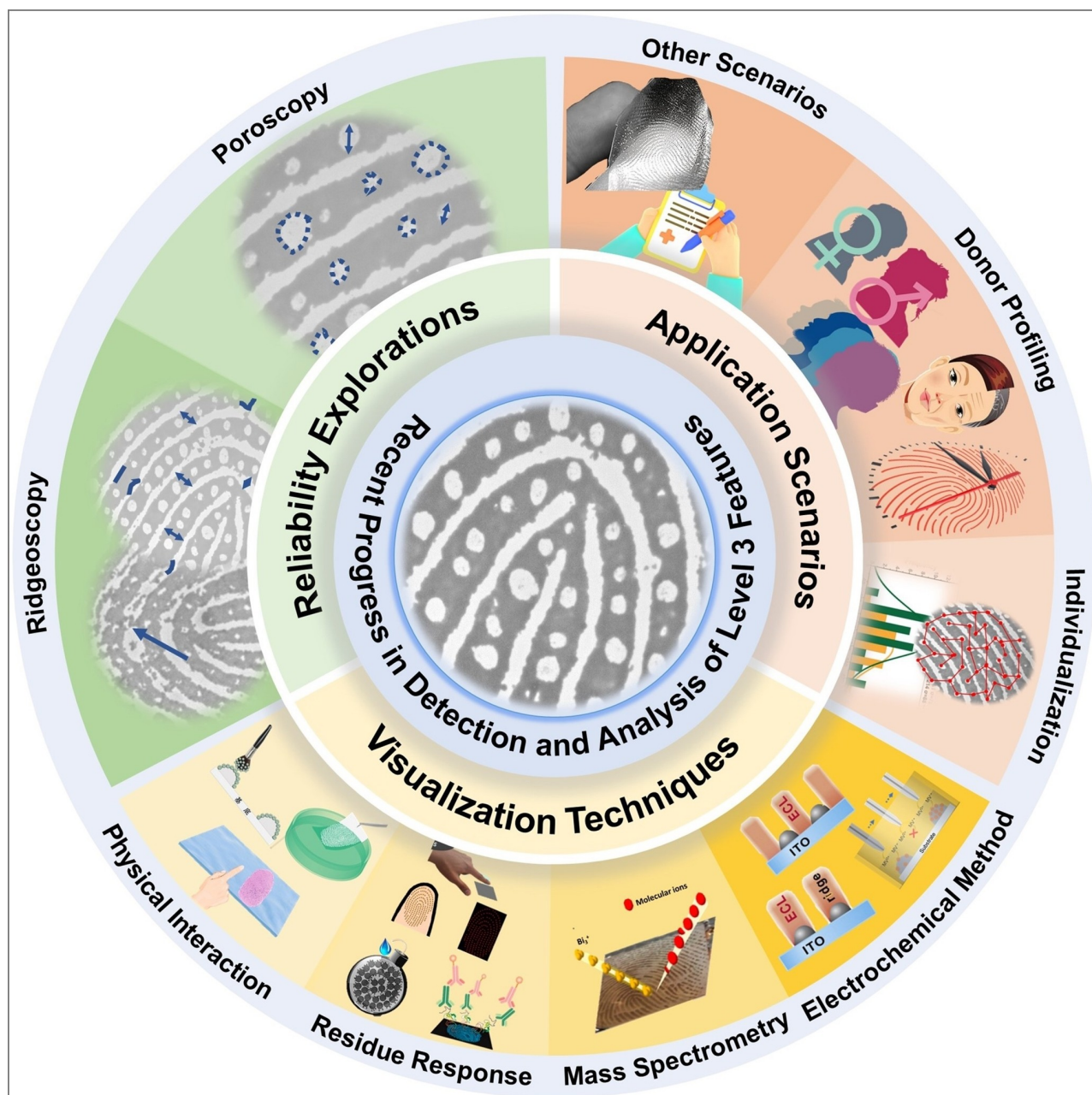Europe
European Chemical
Societies Publishing

www.chemistryopen.org

# Recent Progress in Visualization and Analysis of Fingerprint Level 3 Features

Hongyu Chen,[a] Rongliang Ma,*[b] and Meiqin Zhang*[a]

**ChemistryOpen**

Review
doi.org/10.1002/open.202200091

**Chemistry Europe**
European Chemical
Societies Publishing

Fingerprints provide sufficient and reliable discriminative characteristics which have been considered one of the most robust evidence for individualization. The limitation of current minutiae-based fingerprint technology seems to be solved with the development of level 3 features since they can offer additional information for problematic fingerprint recognition and even donor profiling. So far, tremendous efforts have been devoted to detecting and analysing the third-level details. This review summarizes the advances in level 3 details with an emphasis on their reliability assessment, visualization methods based on physical interaction, residue-response, mass spectrometry and electrochemical techniques, as well as the potentiality for individualization, donor profiling and even other application scenarios. In the end, we also give a personal perspective on the future direction and the remaining challenges in the third-level-detail-related field. We believe that the new exciting progress is expected in the development of level 3 detail detection and analysis with continued interest and attention to this field.

## 1. Introduction

Fingerprints refer to patterns on fingertips with friction ridges and recessed furrows being regularly arranged.[1] They have been regarded as one of the most valuable and solid evidence in court due to their uniqueness, immutability and permanence.[2–4] Fingerprints carry sufficient and reliable discriminative characteristics which ensure the acceptance of fingerprint comparison as a valid individualization method. Generally, fingerprint characteristics are classified into three dimensions, namely level 1, level 2 and level 3 features (Figure 1).[5] Specifically, level 1 features include the macro pattern types and ridge flows, such as loop, whorl, arch and accidental. Level 2 features give details at a deeper scale, termed Galton characteristics or minutiae points (ridge ending, enclosure, bifurcation, hook, eye, etc.). Level 3 features contain all microscopic attribute dimensions of ridges, pores, incipient ridges, warts, creases, scars, etc.[6]

Current fingerprint technology has been developed primarily focused on the first-level and second-level features. As we know, 6–17 minutiae (varying from country to country) guarantee the success of fingerprint recognition.[5] Nevertheless, it is not always satisfactory to process fingerprints by only employing patterns and minutiae points. The main reason lies in that fragmentary or deformed fingerprints are frequently met at crime scenes.[7] When comparing these problematic fingerprints against the prints in a database, their insufficient characteristics may cause fingerprint mismatch and thus reduce the discrim-

inatory power. Moreover, fingerprints found in practice are often invisible, which are called latent fingerprints (LFPs) and needed to be visualized before conducting recognition.[8] It has to be pointed out, conventional fingerprint treatments may cover details and even result in pseudo characteristics, that decrease the identification accuracy. In addition, fingerprints and their level 1–2 details can be easily faked by molding methods or inkjet printing methods.[9–11] Thus, spoof and real samples are unable to be discriminated through the minutiae-based fingerprint matching system.

Apart from level 1–2 features, level 3 fingerprint features are also permanent, immutable and unique.[12] Back in 1912, Locard proved that 20–40 pores are enough to give a personal identification opinion.[12] From then on, the third-level-feature based algorithms have been proposed and improved the performance of the recognition system to some extent.[13,14] Jain et al. reported that the error matching rate declined by 20% after level 3 features were combined with level 1–2 features.[15] Recent studies indicated the third-level features are useful for obtaining additional information about donor gender, age, race, health, etc. than just individualization.[5] Thus, level 3 details have the potential to offer a new strategy for problematic fingerprint (incomplete, deformed, or forged) recognition and even donor profiling. Unfortunately, the actual usage of level 3 details accounts for less than 1%.[16] Investigating the reason, it is mainly that the current visualization reagents for LFPs or deposition methods cannot well display the third-level structures.[17] Another is that the fingermarks

[a] Dr. H. Chen, Prof. M. Zhang
Beijing Key Laboratory for Bioengineering and Sensing Technology
School of Chemistry and Biological Engineering
University of Science and Technology Beijing
30 Xueyuan Road, Beijing, 100083 (P.R. China)
E-mail: zhangmeiqin@ustb.edu.cn

[b] Prof. R. Ma
Institute of Forensic Science
Ministry of Public Security
Beijing 100038 (P. R. China)
E-mail: marl2013@163.com
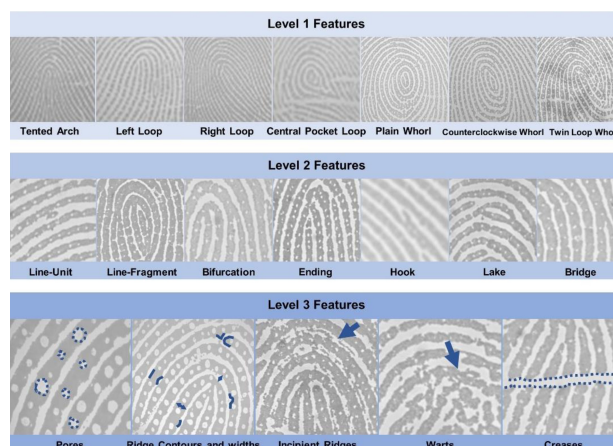
**Figure 1.** Fingerprint characteristics are categorized into three levels.

**ChemistryOpen**

Review

doi.org/10.1002/open.202200091

**Chemistry Europe**
European Chemical
Societies Publishing

left at crime scenes usually have poor quality, whose level 3 features are insufficient for the following identification procedure. Besides, fingerprint images are routinely captured at the resolution of 500 pixels per inch (ppi) which cannot meet the standards ($\geq 1000$ ppi) of third-level feature extraction.[18] Last but not least, no systematic analytical methods for level 3 features have been established at home and abroad. Although high-resolution ($\geq 1000$ ppi) fingerprint imaging techniques have driven the growth of third-level-feature based algorithms, there still exist some challenging issues for improving the comparison accuracy.[13]

The urgent demands for introducing level 3 features into fingerprint recognition and donor profiling have attracted not only forensic experts but also researchers from other fields. To date, considerable efforts have been devoted to detecting and analyzing the third-level details. Therefore, it is necessary to give an overview of the recent advances in level 3 details with an emphasis on their reliability assessment, visualization methods as well as the potentiality for individualization, donor profiling and even other application scenarios. Specifically, four main sections are organized in this minireview. The first part provides a general description of the level 3 feature types and the fundamental studies on their quality and reliability. The second section introduces the multivariate techniques for detecting third-level features involving physical interaction methods, residue-responsive reagents, electrochemical techniques and mass spectrometry (MS) methods. The third part illustrates the application potentiality of level 3 characteristics, particularly in personal identification, donor profiling, fingerprint age determination, spoof fingerprint differentiation and even disease diagnosis. In the last part, the future directions of level 3 details detection and analysis are also outlined followed by a summary.

## 2. Reliability of Level 3 Features

Perception varies widely about which details fall into the level 3 categories.[19] Adopting such a view that level 3 features are everything except the fingerprint flows, patterns and minutiae points, incipient ridges, warts, creases and scars are considered as the third-level characteristics. However, Champod holds that they should be ascribed to level 2 features because they don't require further magnification to be recognized.[20] Actually, level 3 features involve all microdimensional attributes of a ridge. Under this perspective, the incipient ridges, creases, and scars belong to level 3 features only when we focus on their microscopic details such as size, shape, length, width, angle, etc. Beyond the above controversial features, the ridge contour and width (termed ridgeoscopy), as well as pore shape, size, location, frequency and interspace (termed poroscopy), are also included in the third-level features. Note that only employing level 2 details is incapable of problematic fingerprint comparison (fingerprints with low quality or spoof fingerprints), many researchers turn to explore the evidentiary power of level 3 details.

Nonetheless, level 3 details are easily affected by multiple factors, such as the physical conditions of donors, deposition conditions, storage circumstances, etc.[21,22] Hence, it is essential to clarify the reliability of level 3 features under various conditions. Generally speaking, reliability can be assessed by reproducibility and persistency, that is, whether level 3 details can be reproduced in several depositions or over a time interval.[22] Given that poroscopy and ridgeoscopy have been broadly discussed in many publications, we primarily introduce the reproducibility and persistency of the above two features followed by a detailed summary table (Table 1).
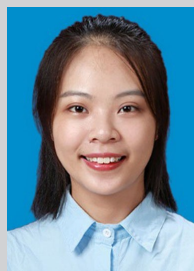
Hongyu Chen received her masters degree in Forensic Science at Criminal Investigation Police University of China in 2020. She is now a PhD student at School of Chemistry and Biological Engineering, University of Science and Technology Beijing. Her research interests mainly focus on the visualization and analysis of multidimensional information in latent fingerprints such as level 3 features, endogenous/exogenous fingerprint residues, donor profiling, fingermark age and DNA profiles.

Rongliang Ma is now a professor at Institute of Forensic Science, Ministry of Public Security in Beijing. He studied at Centre for Forensic Science, University of Technology Sydney (UTS), Australia and received his PhD from UTS in 2012. His research interest and activities include the detection of latent fingermarks, the practice and theories of fingerprint identification and Automated Fingerprint Identification System (AFIS), and fingerprint intelligence. He is a member of the Interpol AFIS Expert Working Group and the Chair of Fingerprint Workgroup (FW) of Asian Forensic Science Network (AFSN). He is also an adjunct professor of several Chinese Universities.

Meiqin Zhang is currently a professor at University of Science and Technology Beijing. After a PhD at Peking University in 2006, she pursued her research as a postdoc at the Ecole Polytechnique Fédérale de Lausanne (Switzerland) from 2006 to 2007 and a researcher of 'Marie Curie Incoming International Fellowship' at the University of Warwick (UK) from 2007 to 2009. Her research activities include electrochemistry at liquid-liquid interfaces, latent fingerprints development and imaging, development and application of scanning electrochemical microscopy.

**ChemistryOpen**

Review
doi.org/10.1002/open.202200091

**Chemistry Europe**
European Chemical
Societies Publishing

**Table 1.** Reliability of level 3 features.

| Level 3 details | | Persistency[a] | Reproducibility[b] | |
|---|---|---|---|---|
| Poroscopy | Shape/area/size | • One hour (+)[18]<br>• One month (−)[18]<br>• 10 days (−)[28]<br>• 30 days (−)[27]<br>• 48 years (−)[26]<br>• 29 years (−)[33] | Capture methods | • High-quality inked prints (+); Latent prints (−); Livescan prints (−)[24]<br>• inked prints (−): The pore size decreased with the ink amount pressure increasing. [21]<br>• Livescan prints over one hour (+)while over one month (−)[18] |
| | | | Visualization methods | • Cyanoacrylate (−); Ninhydrin (−)[16]<br>• Membrane-water method (−)[30] |
| | | | Deposition pressures | Variable: The pore size decreased with the deposition pressure increasing. [21] |
| | | | Substrate types | • Paper substrates: Glossy paper (−) > Matt paper (−); Non-absorbant paper (−) > Abosobant paper (−)[25]<br>• Adhesive tapes (−) > Glass substrates (−)[28]<br>• NC membranes (−)[30] |
| | Frequency/number | • 8 hours (+)[34]<br>• one month (−)[33]<br>• 10 years (+)[33] | Capture methods | • Inked prints (−)[24]<br>• Direct photographs (+)[33]<br>• Holographic imaging (−)[33]<br>• Livescan prints (−)[33]<br>• Livescan prints (+)[34] |
| | | | Visualization methods | • Membrane-water method (+)[30]<br>• Powdering (−); Ninhydrin (−); Small particle reagent (−); Cyanoacrylate (−)[34] |
| | | | Deposition pressures | Variable: The pore number decreased with the deposition pressure increasing. [21,33] |
| | | | Substrate types | • NC membranes (+)[30]<br>• Glass (−); Polythene (−); Metal (−); Plastic (−); Paper (−); Ceremic tile (−)[34] |
| | Location/Pore-to-pore distance/Pore-to-pore angle | • 10 days (−)[26]<br>• One month (−) 35<br>• 10 years (+)[33]<br>• 21 years (+)[29]<br>• 48 years (+)[26] | Capture methods | • Relative pore location on the friction ridge of inked prints (−)[35]<br>• Ink prints (+)[26,28,29,32] |
| | | | Visualization methods | • Powdering (+) ; Small particle reagent (+)[34]<br>• Membrane-water method(+)[30] |
| | | | Deposition pressures | 200 g-1000 g (+)[32] |
| | | | Substrate types | • NC membranes (+)[30]<br>• Glass (+); Polythene (+); Metal (+); Plastic (+); Ceramic tile (+)[34]<br>• Adhesive tapes (+) > Glass substrates (+)[28] |
| Ridgeoscopy | Ridge edge | • 3 months (+)[33]<br>• 8 years (−)[33] | Substrate types | NC membranes (+)[30] |
| | Ridge width | 2 months (−)[33] | Substrate types | NC membranes (+)[30] |
| | | | Deposition pressures | Variable: The width increased with the deposition pressure increasing[30,33] |
| | Incipient Ridge | • 2 months (−)[33]<br>• 10 years (+)[33] | Deposition pressures | Variable: The incipient ridges were widening, distorted and even disappeared when applied excess deposition force[21] |

[a] "+" represents the parameter that can be reproduced over a time interval while "−" can not. [b]"+" represents the parameter that can be reproduced under the corresponding factors while "−" can not.

## 2.1. Sweat pores

Sweat pores, distributed along the papillary ridges, are formed by the duct traveling from the dermis to the epidermis. Locard claimed the pores are permanent and vary from one person to another.[12] In general, sweat pore features consist of pore size, shape, location, distribution, frequency and pore-to-pore inter-space. Figure 2 shows the schematic measurements of the sweat pore parameters which are commonly applied in current research. Various attempts have been made to ascertain the reproducibility and persistency of sweat pores under different conditions.

The shape of pores can be square, triangle, round, oval or irregular.[5] It should be noted that the pore shape is usually measured by pore size or pore area. The pore size is commonly 50–265 μm in diameter. Its observed size depends on deposition or detection methods, deposition pressures, perspiration activity and fingerprint donors, etc. Ashbaugh suggested that the pore area wasn't reliable for individualization with no evidence to support his assertion.[23] One study has explored the influence of different detection methods on pore area. It advocated the pore area was unchanged in high-quality inked prints while latent and livescan prints didn't accurately reproduce the pore area.[24] On the contrary, the research studied by Sutton et al. showed that the
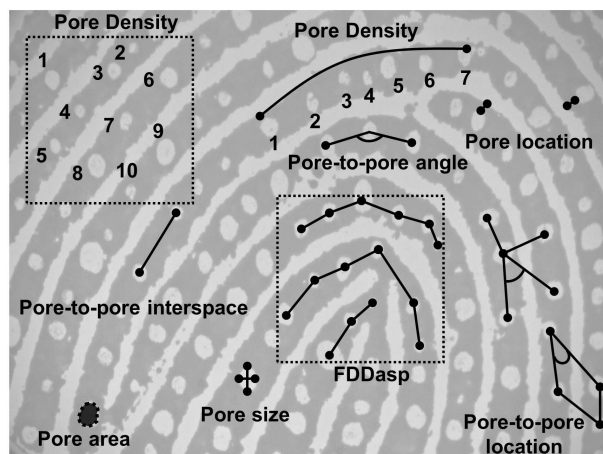
**ChemistryOpen**

Review
doi.org/10.1002/open.202200091

**Chemistry Europe**
European Chemical
Societies Publishing

**Figure 2.** Schematic measurements of sweat pore parameters.

pore area of inked fingerprints was not reliable, independent of the deposition substrate.[25] The group also found the parameter was variable in fingerprints developed using cyanoacrylate or ninhydrin methods.[16] Fu et al. further indicated the pore area of inked fingerprints varied when different ink quantities or deposition pressures are applied. Specifically, the pore size decreased with the ink amount or deposition pressure increasing.[21] The above results demonstrated the ink or conventional visualization methods contributed a lot to the variability of the pore area or size. As the direct microscopic imaging alternative could avoid the deposition effect and physical uncertainty, Sutton's team observed the pore area through direct fingerprint photographs and found the day had a significant impact on pore area measurement.[18] Concretely, the pore area was reproducible over one hour but not for one month. In 2011, Oklevski found the pore size of inked fingerprint samples changed over a dactyloscopy time interval of 48 years, which strengthened the unreliability of the pore area parameter.[26] Cao et al. indicated dynamic changing was individual-dependent and occurred to the sweat pore size along with the epidermal replacement (over 28 days).[27] Dhall et al. later proved the irreproducibility of the pore area over ten consecutive days. Additionally, better pore quality was achieved on the sticky side of adhesive tape than on glass substrates.[28] Recently, Zhou et al. argued that although the collection period affected the pore size, the variation was far less obvious than the changes caused by deposition or detection methods and pressures.[29] Our recent work, published in 2021, also drew the same conclusion that the pore area was subject to high variability in different depositions.[30]

Pore frequency is another feature that fascinated researchers. Locard discovered the pore number may vary from 9–18 pores/cm ridge.[12] Another statistical analysis showed the pore density was 419–519 pores/cm².[24] Gupta's group validated that the pore frequency in the periphery position of fingerprints had a significant correlation in the Index and Ring fingers.[31] The pore impressions may be open in one and closed in the other due to the difference in sweat glands secreting activity, deposition pressure, detection or capture methods, etc. One previous study suggested two inked impressions printed by the same finger displayed a large disparity in pore density.[24] The

reason was explained by Luo et al. and ink deposition can't well reflect the sweat pore number, especially for thick ink printings or donors with small pores.[32] Fu et al. proposed deposition pressure was another factor in that a pore would undergo distortion and stretch to occupy the openings if applied pressure.[21] They found the pore number was well-reflected under low pressure and decreased with pressure increasing. Monson et al. systematically assessed the reproducibility of level 3 details over time by considering the influence of capture methods.[33] In detail, the direct photographs presented the pores whose frequency did not vary even for a ten-year interval, while for holographic or ink rolled impressions, the pore seemed to be obscured over a one-month observation. Additionally, livescan methods failed to display the same level details captured by the other methods, particularly the third level. Singh et al. proposed that the detected pore frequency differed considerably, which depended upon the substrate types that LFPs were deposited on, the enhancement methods that were used for processing LFPs, etc.[34] Besides, the detected number of pores had consistencies with that of the minutiae. Interestingly, livescan prints obtained every hour within eight hours indicated sweat pores didn't periodically close and open. The hypothesis was opposite to previous findings that the closed pore at one stage has been found open at another time point. They proposed the main reason was perhaps not only due to pores' physiology but owning to ink and pressure as well. However, additional experiment data should be presented to draw such a conclusion. The observation interval (one hour) may be too long for pore activity. In other words, the pore activity was unknown during the non-observation period, where sweat pores may periodically close and open. Hence, the pores of live scan prints should be observed within a short interval or real-time monitored. We recently reported the number of sweat pores was consistent with that of the live fingertip and further confirmed the theory of Singh et al. that the presented pore number was the same in several depositions when we eliminated the effects of ink and pressures.[30]

The position of pores was also extensively investigated and inspired high hopes for individualization.[15] It refers to not only the relative location on the friction ridge but also pore-to-pore location, distance, as well as the shape they form together. The pores of inked fingerprints were reported to retain their spatial position relative to one another over 48 years.[26] Luo et al. further emphasized the pore location remained relatively stable with the pressures employed at 200 g, 600 g and 1000 g.[32] Monson et al. validated the pore location captured by direct photographs kept unchanged even for a ten-year interval.[33] The low effect of substrates and development methods on relative pore location was also detected by Singh's group.[34] Zhou et al. subsequently published an article about the reproducibility of pore-to-pore distance and angle over 21 years.[29] Pore-to-pore angle gave an excellent reflection on the location of pore groups and was then proved to be more stable than interspace. Our group compared the frequency distribution of the distance between adjacent sweat pores in three independent depositions, whose results were consistent with earlier research.[30] Very recently, Dhall's team also suggested the pore inter-distance and angle were found to be

reliable and reproducible on glass and adhesive tape substrates.[28] Nevertheless, in the year 2020, Wang et al. discussed the pore location drift over one month. The experiment results demonstrated the pore location observed in either the direct microscopic photography or ink impression suffered the shift in both the longitudinal and transverse directions (maximum up to 166.46 μm, 61.00 μm, respectively).[35] Furthermore, the relative pore location on the friction ridge was found susceptible to the deposition pressure and secreting activity in Cao's work.[27]

## 2.2. Ridge edges, widths and incipient ridges

The level 3 details often have been limited to the consideration of pores, whereas it can be broadened to include shapes of ridge edges, ridge width as well as incipient ridges.[20]

The shape of ridge edges is classified into seven types (straight, convex, peak, table, pocket, concave and angle) by Chatterjee. The diverse shape types are formed by the differential growth of the ridge units and the pores near the ridge edge. After Oklevski examined the 100 pairs of inked impressions, it was detected that the edge feature number decreasing with the capture interval time increasing.[26] The researchers believed the susceptibility of the ridge edges to deformation and damage could account for this observation. Meanwhile, the decline of edge feature quality occurred, where the concave edge features showed the greatest stability. Our findings indicated the ridge shape was well retained on nitrocellulose (NC) membranes with a constant deposition pressure of about 250 g.[30]

Another level 3 parameter involving ridges is supposed to be ridge width which was commonly 200–500 μm.[36] Like edge shape, it was extremely vulnerable to deposition pressures and would become widen if the applied pressing force increased.[21] When the pressure was applied at less than 300 g, ridge width increased significantly, but slowly when pressure was over 300 g.[30] Besides, the variation of ridge width could be negligible by keeping constant press force. Without a doubt, width variation is also possibly attributable to physiological occurrences such as weight gain/loss, usage, gouty deformation, or age.[37]

Incipient ridges located at furrow regions, are generally thinner and lower than papillary ridges and may not be detected in fingerprint impressions.[38] Moreover, they rarely bifurcate and rarely contain pores. Stücker et al. reported that older people (> 20 years old) demonstrated a higher frequency in incipient ridges than the younger group (< 20 years old).[39] In the study published by Silva, the number of incipient ridges increased with age among males.[40] Different from that observed in males, there was a reduction in the number of incipient ridges among older females. Wentworth et al. found no variation was detected in incipient ridges by observing a child's inked impressions collected every two years within ten years.[41] Conversely, Monson et al. obtained a conclusion that incipient ridges of both live fingertips and ink impressions are variable even in a two-month interval.[34] In the year 2013, Fu's group proved the pressure force played role in the reproducibility of incipient ridges. The incipient ridges were

widening, distorted and even disappeared when applied excess deposition force.[21]

# 3. Visualization Techniques of Level 3 Features

Admittedly, the low usage rate of the third-level features is mainly ascribed to unreliable enhancement methods for fingerprints.[17] Specifically, early fingerprint treatments aiming at the extraction of level 1 and 2 details, ignore the significance of the third-level features, which leads to information omissions. Commonly, fingerprints left at crime scenes are invisible to our naked eyes. Although they may carry a certain amount of microscopic features, they will not be detected if no reliable visualization techniques are employed. As mentioned in section 2, there exist considerable level 3 details that can be utilized for problematic fingerprint (recognition and even donor profiling. Hence, researchers are called upon to develop reliable level 3 feature enhancement techniques and subsequent advancements have occurred in this field. Here, we classified the achievements into four categories including techniques based on physical interaction, residue-responsive reagents, mass spectrometry (MS) methods and electrochemical techniques. As a note, only the methods which can accurately and reliably detect level 3 features will be involved in this section. To get an intuitive insight into the advances, a summary table is presented in Table 2.

## 3.1. Techniques based on physical interaction

### 3.1.1. Techniques based on electrostatic adsorption

With the implementation of nanotechnology over recent years, fingerprint enhancement especially for the third-level details has taken a step forward owing to the excellent physical and electronic properties of various nanomaterials.[42–44] Particularly, quantum dots (QDs) with good performance have been reported to allow LFP imaging with high contrast.[45,46] In the year 2017, Wu et al. utilized red-emitting N-acetylcysteine-capped CdTe QDs (N−L-Cys-capped CdTe QDs) reagent to visualize eccrine LFPs.[7] The fingerprints deposited on aluminium foil were quickly exhibited in about 5 s after being immersed in the as-prepared solution. The numbers of level 3 features such as sweat pores were found accurately mapped and their numbers detected were significantly larger than those processed by the cyanoacrylate agent. However, the reagent was expensive, contained toxic heavy metal ions and was prepared with complicated procedures. More importantly, the level 3 details weren't entirely detected with this QDs-staining method rare-earth doped luminescent nanomaterials are considered to be an alternative for visualizing LFPs on both porous and non-porous surfaces due to their excellent fluorescent property, high chemical stability and high affinity with fingerprint residues.[47,48]

Nagabhushana's group realized the rapid detection of fingerprints using $Sm^{3+}$ doped calcium zirconate nanophosphors ($CaZrO_3$: $Sm^{3+}$) prepared via an environmental-friendly solution combustion route.[47] Notably, the sweat pore shapes of finger-

**ChemistryOpen**

Review
doi.org/10.1002/open.202200091

**Chemistry Europe**
European Chemical
Societies Publishing

**Table 2.** Summary of visualization techniques for level 3 features.

| Techniques | Regent/Mechanism/Material basis | Visualization procedures/Time/Signal | Substrates | Characteristics | Ref. |
|---|---|---|---|---|---|
| Physical adsorption | • N–L–Cys-capped CdTe QDs<br>• Physical adsorption<br>• Eccrine | • Immersing in solution<br>• 5 s<br>• Red fluorescence under 365 nm | Aluminium foil | • Strong emitting light with high contrast<br>• Not all sweat pores can be detected<br>• Toxic, expensive and prepared with complicated procedures<br>• Destructive to samples | 7 |
| | • CaZrO$_3$: Sm$^{3+}$<br>• Physical adsorption | • Powder dusting<br>• Orange-red fluorescence under 254 nm | Glass/Compact disc/Aluminium foil/Pepsi can/Plastic paper/Magazine cover | • Environment-friendly synthesis method<br>• Suitable for various porous and non-porous surfaces<br>• Background hindrance isn't entirely eliminated<br>• Some level 3 features are covered with powder<br>• Destructive to samples | 47 |
| | • LaOF: Pr$^{3+}$<br>• Physical adsorption | • Powder dusting<br>• Red fluorescence under 254 nm | Aluminium foil/Playing cards/Currency notes/Magazine covers | • Environment-friendly synthesis method<br>• Suitable for various porous and non-porous surfaces<br>• Background hindrance isn't entirely eliminated especially for substrates with fluorescence<br>• Some level 3 features are covered with powder<br>• Destructive to samples | 48 |
| | • AIE-TPA-1OH<br>• Hydrophilic-hydrophobic interaction<br>• Sebaceous | • Soaking/Spraying<br>• 30 s<br>• Red fluorescence under 405 nm | Glass/Tinfoil/Steel/Ceramics/Paperboard/Paper/Brick/Wall/Wood/Leather | • Background hindrance is eliminated<br>• Without organic cosolvents and post-treatment steps<br>• Super-resolution imaging (sub-50 nm)<br>• Applicable for multi-substrates, even rough surfaces<br>• Level 3 details weren't available on some substrates<br>• Destructive to samples | 51 |
| | • Membrane-water method<br>• Hydrophilic-hydrophobic interaction • sebaceous | • Put on the aqueous solution/<br>• 1–3 s<br>• Ridge appeared black under transmitting light | NC membrane/Glass slide/Banknote/Coloured paper/Ceramic cup/Palm/Leather | • Fast and simple<br>• No background interference<br>• Suitable for various porous and non-porous surfaces and even problematic surfaces<br>• Reliable extraction of level 3 details<br>• Transferred fingerprints exhibit less level 3 details than fingerprints deposited on membranes<br>• Non-destructive to samples | 6, 52 |
| | • PVA nanopaper<br>• Dissolution effect<br>• Water | • Deposition<br>• 3 s<br>• Ridge appeared black under natural light or light-emitting | PVA nanopaper | • Simple, efficient, and controllable synthesis procedures<br>• No ink required<br>• No discussion on transfer efficiency of nanopaper | 53 |
| | • TPU/fluorescein electrospun mats<br>• Water responsive property<br>• Water | • Deposition/Transferring<br>• 30 s<br>• Red under natural light or black under excitation at 432 nm | TPU/fluorescein electrospun mats/Quartz/Glass/Stainless steel/Polypropylene film/Marble/Wood | • Sensitive and fast<br>• Suitable for various surfaces<br>• Not all sweat pores can be detected<br>• Transferred fingerprints exhibit less level 3 details than fingerprints deposited on membranes | 55 |

**ChemistryOpen**

Review
doi.org/10.1002/open.202200091

**Chemistry Europe**
European Chemical
Societies Publishing

**Table 2.** continued

| Techniques | Regent/Mechanism/Material basis | Visualization procedures/Time/Signal | Substrates | Characteristics | Ref. |
|---|---|---|---|---|---|
| Residue-responsive reagents | • PDA-coated PET film<br>• Water responsive property<br>• Water | • Deposition<br>• $< 20$ μs<br>• Red fluorescence under excitation at 510–550 nm | PDA-coated PET film | • Sensitively map and reproduce the sweat pores<br>• Differentiate the active pores and inactive pores<br>• Requires tedious screening of diacetylene monomers and hygroscopic elements<br>• Unstable in humid environments (relative humidity over 80%)<br>• Expensive<br>• Not suitable for old fingerprints<br>• No discussion on the transfer efficiency<br>• Only offer pore information | 56 |
| | • Fluorescein-PVP film<br>• Water responsive property<br>• Water | • Deposition<br>• 1–10s<br>• Green fluorescence under excitation at 460–490 nm | Fluorescein–PVP film | • Sensitively map and reproduce the sweat pores<br>• Differentiate the active pores and inactive pores<br>• Stable in humid environments (20–90%)<br>• Cost effective<br>• Not suitable for old fingerprints<br>• No discussion on the transfer efficiency<br>• Only offer pore information | 57 |
| | • DA-1-derived PDA-coated paper<br>• Water responsive property<br>• Water | • Deposition<br>• Red fluorescence under excitation at 510–550 nm | DA-1-derived PDA-coated paper | • Sensitively map and reproduce the sweat pores<br>• Differentiate the active pores and inactive pores<br>• Stable in humid environments (20–95%)<br>• Not suitable for old fingerprints<br>• No discussion on the transfer efficiency<br>• Only offer pore information | 58 |
| | • PDA-PEO composite film<br>• Water responsive property<br>• Water | • Deposition<br>• Ridge appeared green under UV excitation at 510–550 nm | PDA-PEO composite film | • Sensitively map and reproduce the sweat pores<br>• Differentiate the active pores and inactive pores<br>• Stable in humid environments (20–95%)<br>• Flexibility and can visualize sweat pores of highly curved skin surfaces<br>• Not suitable for old fingerprints<br>• No discussion on the transfer efficiency<br>• Only offer pore information | 59 |
| | • Supra-CDs Paper<br>• Water responsive property<br>• Water | • Deposition<br>• 5 s<br>• Green fluorescence under UV excitation | Supra-CDs Paper | • Low-toxicity and eco-friendly<br>• Differentiate the active pores and inactive pores<br>• Not suitable for old fingerprints<br>• No discussion on the transfer efficiency<br>• Only offer pore information | 60 |
| | • Ln-MOFs<br>• Water responsive property<br>• Water | • Deposition<br>• 180 s<br>• Magenta fluorescence under 254 nm UV excitation | Ln-MOFs filter film | • Offer not only pore information but levels 1–2 features<br>• Superior sensitivity to the water molecules.<br>• Long response time<br>• Not suitable for old fingerprints<br>• No discussion on the transfer efficiency | 61 |

**ChemistryOpen**

Review
doi.org/10.1002/open.202200091

**Chemistry Europe**
European Chemical
Societies Publishing

**Table 2.** continued

| Techniques | Regent/Mechanism/Material basis | Visualization procedures/Time/Signal | Substrates | Characteristics | Ref. |
|---|---|---|---|---|---|
| | • PVA/microrods membrane<br>• Phosphate responsive property<br>• Phosphate | • Deposition<br>• 3 s<br>• Blue fluorescence under 365 nm UV excitation | PVA/microrods membrane | • Sensitive and fast<br>• Not all sweat pores can be detected<br>• No discussion on the transfer efficiency | 63 |
| | • Antibody reagents<br>• Antigen-antibody interaction<br>• Keratin 1/10/Cathepsin-D/Dermcidin/HAS/EGF/HBD-2 | • Incubation<br>• Commonly 1 h for porous surfaces while 1 d for non-porous<br>• Ridge appeared black/brown under natural light or emitting red/green/blue fluorescence depending on the tagged secondary antibody | PVDF membrane/NC membrane/Copy paper/Thermal paper/Aluminium foil/Stainless steel/Plastic sheets/Tile/Bag/Chipboard | • Suitable for non-porous, semi-porous and porous surfaces<br>• Compatible with a wide variety of fingerprint developers<br>• Compatible with DNA analysis<br>• Can realize multiple immunolabeling<br>• Provide additional chemical information than just identification<br>• Long incubation time (15 min–1 d)<br>• Require complex pre- and post-treatments<br>• Destructive to samples | 65–73 |
| | • Aptamer-based methods (Au/pNTP/SiO$_2$ SERS nanoprobes)<br>• Aptamer recognition<br>• Lysozyme | • Incubation<br>• 16 h<br>• SERS signal | Glass/Petri dish/PVDF | • Provide additional chemical information than just identification<br>• Without complicated pre-or post-treatment<br>• Simple, cost-effective, non-destructive, high-resolution<br>• Long incubation time | 74 |
| MS spectrometry | • Combined optical and MALDI-MS Imaging<br>• Na$^+$, K$^+$, urea, amino | • Coating Au LFPs by magnetron sputtering<br>• A few minutes<br>• m/z signals | Glass slides/Membranes | • High-spatial resolution<br>• Faster than full scans with MALDI imaging<br>• Only a limited amount of data from the most interesting areas<br>• Challenging to assign selected signals to physiological substances<br>• Destructive to samples | 75 |
| | • MALDI-ToF/ToF NIMS<br>• BDDA, behentrimonium, DDA, linoleic, oleic, stearic, cholesterol, wax esters, triacylglycerols | • Sputter Coating Ag before fingerprint deposition<br>• m/z signals | Porous silicon wafer | • Maintain resolution because fingerprints are deposited after Ag layer coating<br>• Improve MS mass accuracy<br>• Limited substrate<br>• Limited imaging region<br>• Long scanning time<br>• Destructive to samples | 76 |
| | • ToF-SIMS<br>• Na$^+$, K$^+$, Cl$^+$, SO$_4^{2-}$, SO$_3^{2-}$, H$_2$PO$_4^{2-}$, C$_3$H$_3^+$, C$_3$H$_8$N$^+$, Ca$^{2+}$, C$_{12}$H$_{25}$SO$_4^-$, glycerol, PDMS | • Can pre-treated with conventional methods<br>• 150 min for 18 mm×18 mm region<br>• m/z signals | Stainless steel/Aluminium foil/Glass/Grenade Handle/Silicon wafer/RMB note | • High-spatial resolution<br>• Less destructive<br>• Long scanning time<br>• Limited imaging region | 77, 79, 80 |
| | • GO-enhance ToF-SIMS<br>• Poison, alkaloids controlled drugs, antibiotics, Na$^+$, K$^+$ | • Deposition/Transference<br>• 2 h per image acquisition<br>• m/z signals | Glass/Stair railing/Silicon wafer/GO layer | • Sample on longer limited to the volume of SIMS vacuum chamber<br>• Could be transferred by GO layer<br>• Long scanning time<br>• Limited imaging region | 78 |
| Electrochemical methods | • ECL<br>• Sebaceous residues | • Apply a potential and use the electrochemiluminescent molecule<br>• Electrochemiluminescence signals | ITO glass/Stainless steel | • No pre-treatment<br>• Rapid and sensitive imaging<br>• Spatial selectivity<br>• Less destructive<br>• Restricted to the conductive substrate<br>• ECL decays in 40 s | 82, 83 |

ChemistryOpen

Review
doi.org/10.1002/open.202200091

Chemistry
Europe
European Chemical
Societies Publishing

**Table 2.** continued

| Techniques | Regent/Mechanism/Material basis | Visualization procedures/Time/Signal | Substrates | Characteristics | Ref. |
|---|---|---|---|---|---|
| | • SECM<br>• Sebaceous residues (Lipid oxide) | • Apply a potential and use the electrochemical mediator<br>• Faradaic current | NC membrane/Glass | • Label-free, no pre-treatment<br>• Avoid the background interference<br>• Provide the chemical information of residues<br>• Restricted to the conductive substrate<br>• Long scanning time<br>• Limited imaging region<br>• Non-invasive scanning | 3 |

prints on the glass, namely circle, triangle, open, etc. could be obviously identified. Unfortunately, this nanophosphor seemed to have no contribution to eliminating background interference and could cover the level 3 details when being excessively used. Later, this group adopted $Pr^{3+}$ activated LaOF nanophosphors (LaOF: $Pr^{3+}$) for imaging level 3 structures.[48] They fabricated alkali metal ions blended LaOF: $Pr^{3+}$ via the eco-friendly ultrasound-assisted sonochemical method and the as-obtained product emitted bright red light under 254 nm UV light. Both the open and closed sweat pores were then detected in revealed fingerprints by SEM examination. Inevitably, it should be noted that the background hindrance could be eliminated except for substrates with background fluorescence. However, the powder reagent may adhere to pore regions due to its nonselective physical adsorption visualization mechanism. Moreover, the powder particles especially those at the nanoscale easily aggregate to a larger size which will result in the distortion of level 3 features. Additionally, the fingerprint brush could damage the fingerprint ridges during the visualization process. As a result, the powder may cover or damage some microscopic details and even cause pseudo characteristics.

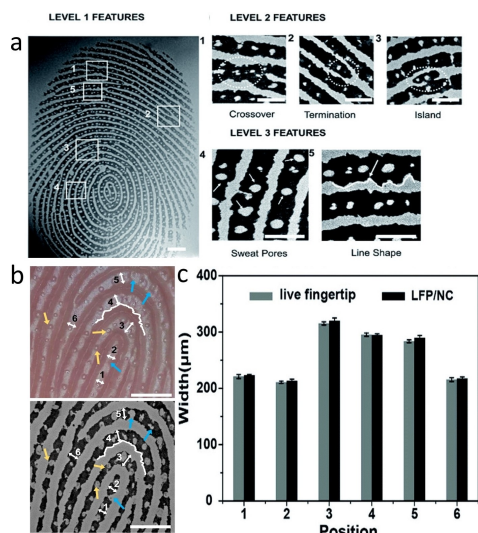### 3.1.2. Techniques based on hydrophilic-hydrophobic interaction

Aggregation-induced emission (AIE) materials have drawn extensive interest for wide applications owing to their colourful fluorescence with high contrast, low toxicity and easy functionalization. Since 2012, they have been employed to reveal LFPs along with limitations discovered in practice: (i) Organic solvents used will do damage to residues while powders harm the forensic technicians; (ii) there exist post-treatments after fingerprint visualization, such as removing excess dye with water or air; (iii) they are customarily suitable for non-porous substrates; and (iv) most dyes are excited under 365 nm light, which will cause damage to the technicians and fingerprint residues such as DNA.[49,50] To address the problems above, an AIE-based water-soluble probe, TPA-1OH was designed without any cosolvent and stabilizer which could emit strong red fluorescence under visible light excitation (405 nm).[51] Its amphiphilicity made it possible to adhere to fingerprint residues through hydrophobic-hydrophobic interaction between the lipophilic end of TPA-1OH and the lipid secretions. Moreover, the electrostatic interaction between the positively charged TPA-1OH and the negatively charged residues was also

helpful for fingerprint enhancement. As depicted in Figure 3, the sweat pores with a diameter of 80–120 μm were found to distribute periodically along the ridges with 100–200 μm interspace. Noteworthily, the detected pores and ridge shapes were consistent with those of live fingertips.

Besides AIE materials, there still exist other methods whose reagents can interact with fingerprints through hydrophilicity or hydrophobicity. In the year 2017, our group developed a fast and reliable visualization method using hydrophilic cellulose membrane and dye aqueous solution.[52] The LFPs deposited on various substrates could be detected through the pre-treatment of membrane transference. In this approach, when the fingerprint/membrane samples were put onto the solution, the relatively hydrophobic fingerprint residues acted as a "mask" which directed dye aqueous solution to occupy the furrows and bare membrane other than ridges. Recently, we developed the sebaceous LFPs deposited on NC membranes with only water, and then the high-resolution optical micrographs were captured.[30] From the picture in Figure 4(a), level 3 features, including all dimensional attributes of the ridges and pores can be accurately and reproducibly extracted. Additionally, the third-level details of water-developed fingerprints, especially pores, ridge contours and widths, were one-to-one matched to those of live fingertips (Figure 4(b)–(c)). Unfortunately, using NC membranes to lift fingerprints on problematic substrates such as skin exhibited fewer level 3 details than those directly deposited on NC membranes.[3]
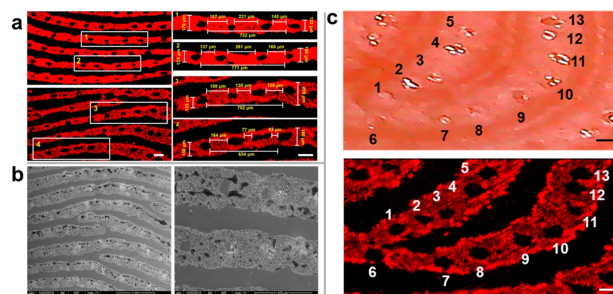


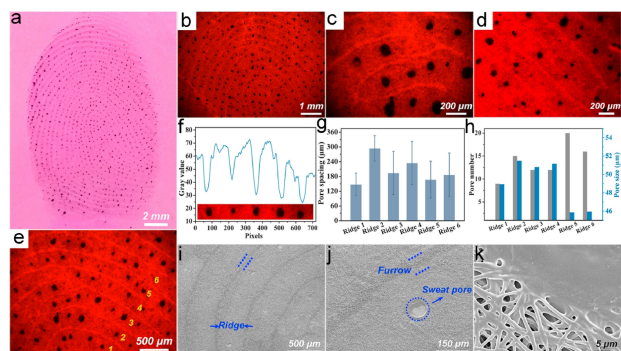**Figure 3.** (a) Fluorescence microscopic images for the partial region of LFPs and the analysis of level 3 microscopic details. (b) SEM images of the fingerprint. (c) Number and location distribution of sweat pores on the bifurcation of the live fingerprint (top) and its developed fingerprint (bottom). Scale bars: 100 μm. Reproduced from Ref. [51] Copyright (2020), with permission of the American Chemical Society.

**ChemistryOpen**

Review
doi.org/10.1002/open.202200091

**Chemistry Europe**
European Chemical
Societies Publishing

**Figure 4.** (a) Optical micrographs for water-revealed LFPs on NC membranes. Scale bars: 1000 μm in level 1 features, 500 μm in level 1 and level 2 features. (b) A direct microscopic image of a live fingertip (top) and a developed sebaceous LFP of the same fingertip on the NC membrane (bottom). The sweat pores in the yellow arrows are showing higher perspiration activities than those in the blue arrows. Scale bars: 1000 μm. (c) Dimension (marked with white double-headed arrows) comparison of the live fingertip and water-developed LFP/NC. Reproduced from Ref. [30] Copyright (2021), with permission of the Royal Society of Chemistry.

### 3.1.3. Techniques based on dissolution effect

Poly (vinyl alcohol) (PVA) materials whose properties are in favour of fingerprint preservation have attracted forensic researchers' attention. An article published in 2020, described a super-soft and water-sensitive PVA electrospun nanopaper for in situ mapping the entire fingerprint characteristics at three levels (Figure 5).[53] The nanopaper possessed two properties that guaranteed the successful detection of fingerprint details: (i) Ultra-softness. Once deposited on the paper, the friction ridge contacted area would be stacked while the furrow regions that didn't touch the paper
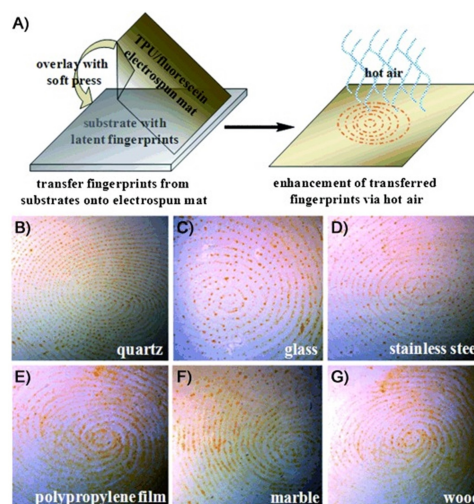
would maintain fluffy; (ii) water sensitivity. A tiny amount of sweat secreted through pores could quickly and selectively dissolve the nanopaper and thereby achieved sweat pores mapping. As shown in Figure 5(g)–(h), a systematic statistic was also conducted in this work. The results demonstrated the pore-to-pore distance ranged 140–300 μm and the pore sizes were about 45–52 μm. As this method exhibited excellent performance, it is urgent to discuss whether the PVA nanopaper can transfer fingerprints on various substrates.

### 3.2. Techniques based on residue-responsive reagents

Endogenous fingerprint residues are mainly secreted by exocrine sweat glands and sebaceous glands including water, inorganic salts, amino acids, polypeptide, proteins, fatty acids, urea, squalene, etc.[54] It is worth noting that all the components can be the foundation of LFP visualization. Particularly, water taking up a very high proportion about 98–99% of eccrine sweat, has led to the emergence of numerous detection methods based on water-responsive reagents.

### 3.2.1. Techniques based on water-responsive reagents

Commercial thermoplastic polyurethane (TPU) resin has a release-induced response (RIR). In the year 2011, Chen et al. prepared TPU and fluorescein (TPU/fluorescein) electrospun mats for facile collection and identification of LFPs on various surfaces.[55] When the water in fingerprint residues contacted the TPU/fluorescein electrospun mat, a crosslinking behaviour between TPU and the residues of fingerprints led to the phase separation between the TPU network and fluorescein. As a result, the fingerprint ridges display an obvious change in color to red. Figure 6 presents the transfer procedure and effective-



**Figure 5.** (a) Optical image of a fingerprint mapped on the PVA nanopaper. (b) Fluorescent image of a fingerprint. (c, d) Level 2 structure (bifurcation, ending). (e) Level 3 structure (sweat pore) of the fingerprint in ridge 1–6. (f) Pixel profile of a small portion of the fingerprint. (g) Sweat pore interspacing, (h) pore size and number in ridge 1–6. (i–k) SEM images of the fingerprint mapped on the PVA nanopaper. Reproduced from Ref. [53] Copyright (2021), with permission of Elsevier.



**Figure 6.** (a) The process for imaging latent fingerprints on various surfaces using the electrospun TPU/fluorescein mat. (b–g) Bright-field images of segmental fingerprints on various indicated surfaces were obtained after heat treatment (100 °C hot air) for up to 30 s. Reproduced from Ref. [55] Copyright (2011), with permission of Wiley-VCH.

ChemistryOpen

Review
doi.org/10.1002/open.202200091

**Chemistry Europe**
European Chemical
Societies Publishing

ness of the TPU/fluorescein electrospun mat for LFPs. The results showed that LFPs could be transferred from various surfaces and quickly developed by heating with hot air (100 °C) in 30 s, which was suited to on-site detection of LFPs. However, the pores and ridge edge of lifted fingermarks seemed poorly enhanced when they were deposited on polypropylene film, marble and wood.

Owing to their hydrochromic property, polydiacetylenes (PDAs) have been actively investigated for applications in humidity monitoring, water content detection of organic solvents, water-jet-based rewritable printing and sweat pore mapping, etc. In the year 2014, Kim and his co-workers reported hydrochromic conjugated polymer (PDA-coated PET film) could map the human sweat pores (Figure 7(a-1)).[56] Intriguingly, a tiny amount of water produced from sweat pores led to a blue-to-red colour change along with the fluorescence emission when the fingertip contacted the as-prepared film. After super-imposing the mapped pores on a fingerprint scanning image, they concluded that the technique could differentiate the activity of sweat pores (Figure 7(a-2)). However, this technique is required to screen hygroscopic elements and diacetylene monomers whose prices were expensive. In addition, the PDA films were too sensitive to enable sweat pore mapping under such environments with relative humidity over 80 %. Subse-

quently, this team designed a new strategy for improving the issues mentioned above. The water-responsive fluorescein and a hydrophilic matrix polyvinylpyrrolidone (PVP) were used for sweat pore detection (Figure 7(b-1)).[57] Fortunately, the cost-effective fluorescein–PVP film was stable in a wide range of humidity around 20–90 %, whereas sensitive to sweat. To further improve the property of hydrochromic films, the imidazolium containing DA monomer (DA-1) was employed by Kim et al.[58] The chemical structure of DA-1 and the stepwise procedure for mapping sweat pores are presented in Figure 7(c). Specifically, the amphiphilic DA-1 could be readily inkjet-printed on conventional paper which subsequently polymerized to PDA after UV-irradiation (30 s) and became blue as well. Once a fingertip pressed on the blue-coloured PDA-coated paper, an immediate colour change from blue to red as well as red fluorescence emission would happen and thus achieve sweat pore mapping on the skin. The colour of as-produced DA-1-derived PDA paper maintained unchanged even in a moisture condition whose humidity was above 90 %. Undoubtedly, the pores distributed in palms, toes and soles were accurately recorded through such a PDA-coated paper. In 2017, this group developed a polydiacetylene-polyethylene oxide (PDA-PEO) composite film, which underwent a blue-to-red colour change once encountered water (a nanolitre of sweat) and successfully achieved human sweat pores imaging.[59] Surprisingly, the flexibility of the PDA-PEO film made it possible to visualize sweat pores of highly curved skin surfaces such as the nose.

Meanwhile, the hydrochromic carbon nanodots (CDs) create another avenue for level 3 details detection because of their unique optical properties. Shen et al. reported a supra-CD pore mapping system by coating supra-CDs self-assembled by dodecyl-functionalized CDs (CD–Ps) on filter paper.[60] Its water-responsive behaviour was ascribed to the decomposition of the supra-CDs when contacting water. Notably, the strong emission of supra CD-coated paper wouldn't be extinguished even after the water evaporated.

Nevertheless, whether the as-obtained material could be used to lift fingerprints on various substrates is still unknown. Moreover, only mapping sweat pores will cause characteristic information missing as sweat pores may vary time-to-time. Lanthanide metal-organic frameworks (Ln-MOFs), ideal candidates for sweat pore mapping, are recently designed by Zhou et al.[61] They converted into magenta light after reacting with water in a response time of 180 s. Although they offer not only pore information but also pattern type and minutiae points, the potential for the practical transference of fingerprints should be included in further investigation.
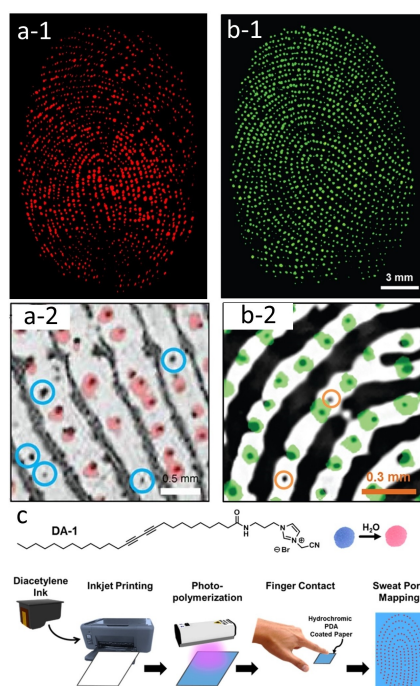


**Figure 7.** (a–b) Contrast-enhanced fluorescence image of a sweat pore pattern mapped on the PDA-coated PET film (a-1) and fluorescein-PVP composite film (b-1). Superimposed image of the fluorescence sweat pores (a-2) and (b-2) on a scanned fingerprint digital image. The black dots inside the circles indicate pores that do not secrete sweat. (a-1) and (a-2) reproduced from Ref. [56] Copyright (2014), with permission of Springer Nature. (b-1) and (b-2) reproduced from Ref. [57] Copyright (2015), with permission of The Royal Society of Chemistry. (c) Schematic illustration of Inkjet-printable imidazolium-modified PDA precursor for sweat pore mapping. Reproduced from Ref. [58] Copyright (2016), with permission of Wiley-VCH.

### 3.2.2. Techniques based on phosphate-responsive reagents

Phosphate (Pi) is rich in eccrine sweat (1.4 mg/L).[62] Huang et al. designed a Pi-responsive PVA electrospun nanofibrous (NFs) membrane where the assembled dual-emission microrods of carbon quantum dots (CQDs) with Eu (III) ion ((CQDs)-Eu (III)) are embedded (PVA/microrods).[63] The preparation procedure and application in fingerprint visualization were demonstrated

in Figure 8. The membrane had strong red emission under UV irradiation due to the aggregation-induced Dexter energy transfer from CQDs to Eu (III) ions. When a fingertip touched the as-prepared membrane, Pi in sweat secretions could bind with the Eu (III) ions and block the Dexter energy transfer from CQDs to Eu (III) ions, leading to the recovery of the blue fluorescence of CQDs. As a result, the ridge-occupied area emitted a blue fluorescence under UV irradiation and even presented the sweat pore distributed along the papillary ridges. The PVA/microrods membrane could be made into paper and enabled to identify the person who touched the PVA/microrods document through fingerprint analysis. Moreover, it would be of additional value if the PVA/microrods membranes were applied to lift LFPs on various substrates.

### 3.2.3. Techniques based on immunolabeling reagents

Besides water, protein and polypeptide, whose content is 150–250 mg/L, have been regarded as the most abundant components in eccrine secretion.[64] To date, a few proteins including albumin, keratins 1/10, cathepsin D, dermcidin, lysozyme and EGF have been identified in fingerprints through various techniques.[1] The level 3 detection through immunolabel method dated back to the year 2009. Drapel and her co-workers used anti-keratin 1/10, anti-cathepsin-D and anti-dermcidin to visualize fingerprints deposited on polyvinylidene fluoride

(PVDF) membranes, non-whitened papers and whitened papers.[65] The experiment results showed the revealed fingerprints on PVDF obtained the best quality. Furthermore, antigens originating from the epidermis gave well-defined ridge edges (keratins 1 and 10; cathepsin-D) whereas antigens secreted by sweat glands offered pore information (dermcidin). The pore mapping presented in Figure 9 was revealed by anti-dermcidin reagents. To enhance the immunodetection signal, visible dyes, organic fluorophores and nanoparticles were later investigated to be tagged to the secondary antibody.[66–70] As a result, the immunolabeling application scenario for various substrates was expanded and subsequently proved to be fitted in DNA analysis.[71] Since the amount of dermcidin secreted is found to be variable and sometimes tiny, multi-target immunolabeling approaches that can simultaneously react with several peptides have exhibited great potential for high-quality pore visualization recently.[72,73]

Compared with antigen-antibody interactions, the aptamer recognition methods open a facile pathway for the detection of level 3 details on account of their exceptionally high specificity and affinity to fingerprint residues. Liu et al. reported a lysozyme-binding aptamer (LBA)-modified sandwich-structured Au/pNTP/SiO$_2$ surface-enhanced Raman scattering (SERS) probe.[74] After SERS imaging, the second and third-level details could be obviously distinguished, especially for eccrine prints on glass substrates (Figure 10). Noteworthily, the Au/pNTP/SiO$_2$-LBA probe deposited on eccrine prints (Figure 10(c)) was more than that on sebaceous prints (Figure 10(d)) indicating the higher content of lysozyme in eccrine secretions.
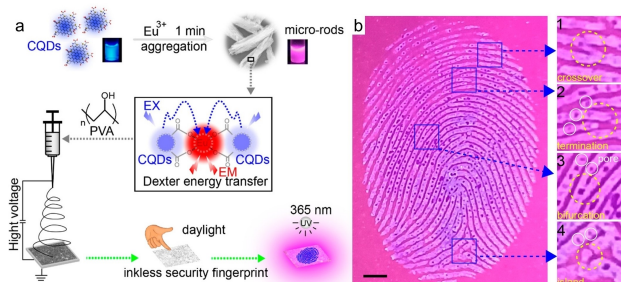


**Figure 8.** (a) Contrast-enhanced fluorescence image of a sweat pore pattern mapped on the PDA-coated PET film (a-1) and fluorescein-PVP composite film (b-1). Superimposed image of the fluorescence sweat pores (a-2) and (b-2) on a scanned fingerprint digital image. The black dots inside the circles indicate pores that do not secrete sweat. (c) Fluorescence images of the PVA/microrods NFs membrane after finger touch. Scale bar: 2000 μm. Magnified images of blue boxes showing level 2 details including crossover (1), termination (2), bifurcation (3), island (4) and level 3 details (pores in 2, 3, and 4). Reproduced from Ref. [63] Copyright (2019), with permission of the American Chemical Society.
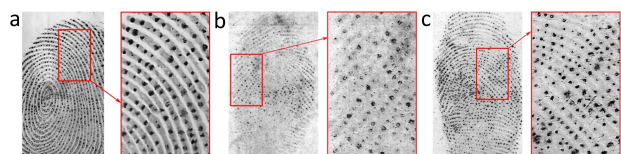


**Figure 9.** Mixed fingerprints were printed on a PVDF membrane (a), a non-whitened paper (b) and a whitened paper (c) which was immunodetected with anti-dermcidin. Reproduced from Ref. [65] Copyright (2009), with permission of Elsevier.
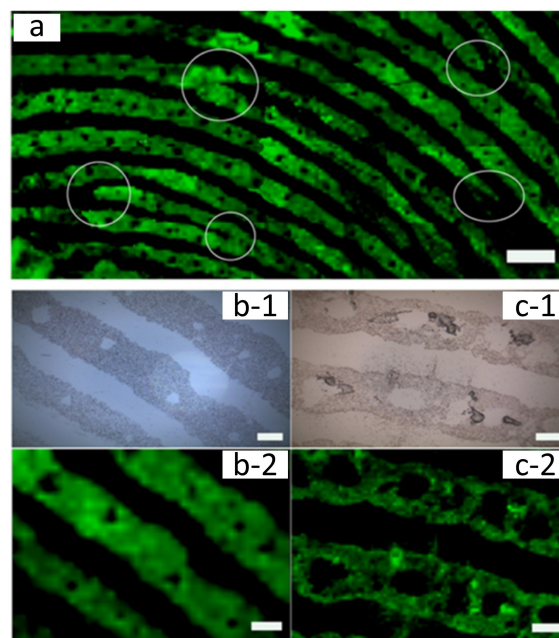


**Figure 10.** (a) SERS imaging of eccrine fingerprints on a glass surface using Au/pNTP/SiO$_2$-LBA nanoprobes. Optical images of eccrine (b-1) and sebaceous (c-1) fingerprints (Scale bar: 120 μm). Corresponding SERS imaging of eccrine (b-2) and sebaceous (c-2) fingerprints (Scale bar: 150 μm). Reproduced from Ref. [74] Copyright (2016), with permission of the American Chemical Society.

ChemistryOpen

Review
doi.org/10.1002/open.202200091

Chemistry
Europe
European Chemical
Societies Publishing

## 3.3. Imaging Mass spectrometry (IMS) techniques

IMS spectrometry has drawn a lot of attention in recognizing and imaging the chemical fingerprint components. Among the numerous mass spectrometry techniques, time-of-flight secondary ion mass spectrometry (ToF-SIMS) and matrix-assisted laser desorption ionization mass spectrometry (MALDI-MS) occupy an absolute advantageous position in sensing level 3 features of fingerprints. Thus, we primarily summarized the two techniques in detail.

### 3.3.1. MALDI-MS imaging techniques

Abel and Elsner utilized a MALDI-MS technique to selectively image the interesting region of LFPs assisted by optical positioning. Promisingly, the whole acquisition time lasted for a few minutes, which was 2–3 orders of magnitude faster than conventional full MS scanning.[75] This combined optical and MS imaging could offer level 1–3 features, not just pore information. Admittedly, it is challenging to assign selected signals to physiological substances of fingerprint residues. One year later, Voelcker et al. employed the MALDI-ToF/ToF MS technique to achieve nanostructural imaging on Ag layers (0.4–3.2 nm) coated porous wafer silicon (Ag-coated pSi). Mass accuracy of this method was improved by more than an order of magnitude and thereby could visualize fingerprints along with their level 3 details.[76]

### 3.3.2. ToF-SIMS imaging techniques

ToF-SIMS has superior spatial resolution and do less destruction to fingerprint samples than the MALDI-MS imaging technique. It was initially introduced by Bailey et al. with a discussion about the feasibility of fingerprint detection using such mass spectrometry method.[77] The three scenarios illustrated by this group delivered a good signal that fingerprints could be enhanced using ToF-SIMS even for those which were poorly developed with conventional methods. In the year 2017, Graphene oxide (GO)-enhanced ToF-SIMS was reported to detect poison, alkaloids ($>600$ Da) and controlled drugs, and antibiotics ($>700$ Da) of relatively high mass molecules in contaminated fingerprints as well as endogenous substances ($Na^+$, $K^+$).[78] Delicate fingerprint characteristics reaching the third level are obtained as presented in Figure 11. The pore sizes, shapes and distribution could be clearly observed. The pore in Figure 11(d) was a triangle whilst seemed round in Figure 11(e). Another group then attempted to broaden its application to fingerprints left on the stainless steel. Results showed it was capable of identifying pore level details even for those who were deposited for 26 days.[79] Very recently, Li's group has attempted to image fingerprints on banknotes according to the signal molecular ions and fragment ion peaks of both endogenous chemicals and contaminants.[80] Certainly, the pore structure could also be captured rough substrates more than smooth surfaces. Although the methods mentioned
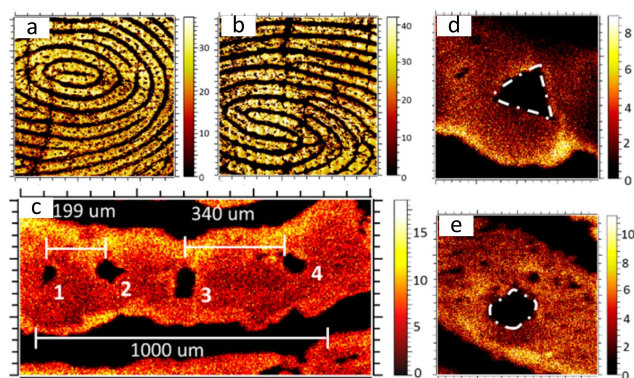


**Figure 11.** 2D SIMS images of molecular ions of roxithromycin at m/z 837.5 in fingerprints contaminated by roxithromycin solution. (a, b) Scan area: 5000×5000 μm² in MacroRaster mode, 128×128 pixels. (c) Scan area: 1200×600 μm² in MacroRaster mode, 128×128 pixels. (d, f) Scan area: 400×400 μm², 256×256 pixels in normal 2D mode. Reproduced from Ref. [78] Copyright (2017), with permission of the American Chemical Society.
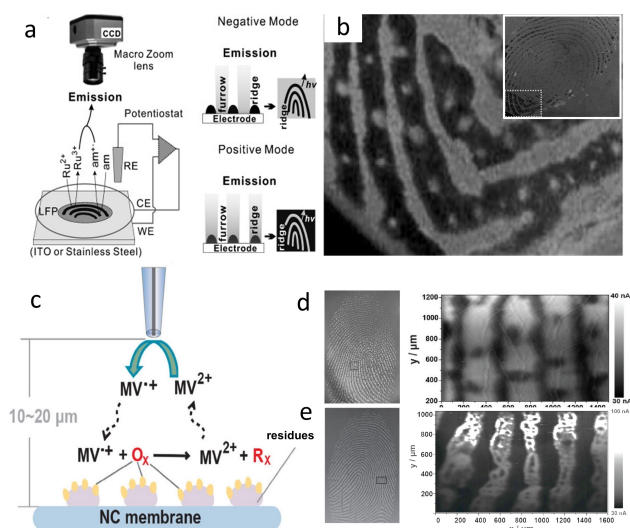
have exceptional performance in sweat pore detection, the long scanning time might hinder the implementation in forensic investigation practice.

## 3.4. Electrochemical techniques

Over the past two decades, unavoidable background interference has driven the development of electrochemical methods for fingerprint imaging. Intriguingly, two methods, electrochemiluminescence (ECL) and scanning electrochemical microscopy (SECM) techniques have already been reported to accurately and reliably visualize level 3 features owing to their sensitivity, good controllability and low toxicity.[81] Below is the achieved progress in the imaging of third-level characteristics through those methods.

### 3.4.1. Fingerprint level 3 detail imaging by ECL

ECL is commonly generated by certain electrochemical reactions triggered by a potential. Su's group pioneered the application of ECL to fingerprint visualization in 2012.[82] In principle, the sebaceous residues of fingerprints on conductive substrates act as a mask or template. By spatially controlling the ECL reactions to occur in either the bare surface or ridge-occupied area, the negative mode and positive mode of fingerprint imaging can be obtained (Figure 12(a)). As demonstrated in Figure 12(b), the sebaceous fingerprints of seven months old could be clearly visualized with partial sweat pores located along the ridges. They also performed ECL by using a highly electrochemiluminescent molecule, namely rubrene. In positive mode, the papillary ridges illuminated ECL with the dark background, eventually generating a fingerprint impression whose level 3 features could be identified.[83] Although ECL is rapid and sensitive for imaging LFPs, it is restrictive to only conductive substrates.

**ChemistryOpen**

Review
doi.org/10.1002/open.202200091

**Chemistry Europe**
European Chemical
Societies Publishing

**Figure 12.** (a) Schematic representation of ECL imaging principle of two modes. (b) Magnified ECL images of a seven-month-old sebaceous fingerprint on an ITO electrode. Reproduced from Ref. [82] Copyright (2012), with permission of Wiley-VCH. (c) Schematic representation of SECM imaging principle for label-free LFP/NC using methyl viologen. (d, e) SECM imaging for a sebaceous LFP directly left on NC membrane (d) and lifted by NC membrane (e). Reproduced from Ref. [3] Copyright (2020), with permission of Elsevier.

### 3.4.2. Fingerprint level 3 detail imaging by SECM

SECM has been successfully applied to electrochemical image substrate topography and local reactivity with high resolution. It has been proven by Girault's group that silver-stained proteins on PVDF membranes can be visualized by recording the tip current signal generated by the oxidation of the mediator $K_3IrCl_6$.[84] Afterward, this group initially performed SECM imaging on silver-stained fingerprints. Satisfactory results were obtained despite excessive silver staining and feature being covered.[85] Our group has been working on label-free fingerprint imaging using SECM without pre-treatment procedures, such as silver-staining.[3] Theoretically, the mediator methyl viologen could selectively react with the electroactive species residues rather than furrow regions, resulting in the sharp contrast current change between ridges and furrows. Figure 12(d) and (e) illustrate the feasibility of this label-free method for visualizing level 3 details. More interestingly, the fingerprints deposited on other surfaces such as glass could be imaged after conducting the membrane-lifting procedure. Additionally, the imaging time could be reduced if we combined optical microscopy methods once fingerprints were transferred by the NC membrane.

## 4. Applications of Level 3 Features

With the rapid development of level 3 detail imaging techniques, tremendous interest has been aroused in exploring potential applications of revealed level 3 details. So far, many articles have demonstrated they are not only useful for individualization,

particularly in fragmentary fingerprints, but also provide valuable information about donor profiling, fingerprint age determination, spoof fingerprint differentiation, as well disease diagnosis. In this section, we give a brief introduction to the applications that have already been investigated and then provide a detailed summary in Table 3. It should be pointed out that the involving matching algorithm details of application in personal identification will not be included in this section as many reviews have already covered this part.[86]

### 4.1. Individualization

There is growing interest in utilizing level 3 details for fingerprint recognition, especially for those with fragmentary impressions. Jain et al. indicated that the error matching rate declined by 20% when combining level 3 features with levels 1–2 features.[15] Among the various level 3 features, pores have received huge attention. Back in 1912, Locard claimed that 20–40 pores are enough to give a personal identification opinion.[12] From then on, many pore-based matching algorithms emerged as the implementation of high-resolution fingerprint images..[13–15,56–58,87–89] Since pore shapes and sizes vary from one impression to another, the pore position is mostly used in fingerprint matching and improve the comparison accuracy to some extent. Current pore-based fingerprint comparison systems mainly rely on two algorithms: alignment-based pore comparison algorithm and direct pore (DP) comparison algorithm.[13] Unfortunately, pore comparison is still a challenging issue because the pore alignment accuracy and only local feature extraction heavily affect the comparison result.[13] Additionally, a very limited number of studies focused on other types of level 3 features have also been reported. Jorgenson reported one fingerprint with a limited number of minutiae (3–5 minutiae) was successfully identified by a combination of shapes of edges and minutiae.[90] Reneau then published a case where a fingerprint with no minutiae was differentiated through edge shapes and secondary ridges matching.[91] Meanwhile, substantial efforts were devoted to exploring algorithms relying on ridge counter, incipient ridge, and creases.[15,92–95]

Our group recently proposed a new parameter termed "frequency distribution of the distance between adjacent sweat pores" (FDDasp), which was used for describing the pore-to-pore location.[30] The parameter was highly identifiable and thus applied to differentiate two fingerprint fragments whose minutiae were the same. As Figure 13 illustrated, the pore-to-pore distances of the two fragments were not consistent. In combination with other characteristics such as edge shape, we ultimately gave an opinion that the fingerprints were from different fingertips. In the future study, more fingerprint samples should be included to further verify the identifiability of the proposed parameter. Meanwhile, larger area of one fingerprint sample should be statistically explored such as the FDDasp in different regions of the same fingerprint.

**Table 3.** Recent advances in the application of level 3 features.

| Applications | Parameter | Outcome |
|---|---|---|
| Individualization | • Pore location<br>• Ridge edgers, incipient ridges, creases, scars | • 20–40 sufficient for identification<br>• Accuracy has been improved[15,56–58,87–95] |
| | FDDasp<br>(Pore-to-Pore distance) | Differentiate two fingerprint fragments whose levels 1–2 features are the same[30] |
| Donor sex | Pore frequency | • No significant difference:<br>Male: 8.40 pores/cm ridge; Female: 8.83 pores/cm ridge[96]<br>• Significant difference:<br>Male: $\leq 32$ pores/cm$^2$; Female: $\geq 36$ pores/cm$^{2[97]}$<br>• No significant difference:<br>Male: 2–4 pores/cm ridge; Female: 2–4 pores/cm ridge[98] |
| | Pore size | • No significant difference:<br>Male: 69–284 μm; Female: 66–287 μm[96]<br>• Significant difference:<br>The pore size of males is larger than that of females[27] |
| | Pore shape | • Significant difference:<br>Circular or round pores possessed higher occurrence in males than females[98]<br>• No significant difference[97] |
| | Pore location shift | • Significant difference (longitudinal and transverse location shifts):<br>Male: 166.46 μm and 61.00 μm; Female: 73.08 μm and 45.88 μm[99] |
| | Ridge shape | • Significant difference (sample number of 1 concave in 1 cm ridge):<br>Male: 160 out of 200; Female:126 out of 200[100] |
| Donor age | Pore type | Significantly different in males:<br>The closed pore number decreases with age advanced[96] |
| | Pore shape | Significantly different in males:<br>The circular pores decrease and the oval pores increase with age advanced[96] |
| | Pore size | Significant differences:<br>The pore size increase with age advanced[96] |
| Group | Pore size | Racial: There is a difference in the pore size of Brahmins and Rajput's of Himachal Pradesh[101] |
| | Ridge width | Criminals: Ridge width of eleven criminals was found to vary in right and left hands while no significant differences were detected in normal people[102] |
| Fingerprint age | Ridge width | Ridge suffered narrowing and a loss in the ridge continuity over time[104] |
| Others | Pore | • Spoof fingerprints differentiation:<br>Pore numbers differ in spoof and genuine fingerprints[30]<br>• Disease diagnosis[106,107] |

## 4.2. Donor profiling and fingerprint age determination

Fingerprint level 3 details offer additional information than just identification such as donor gender, donor age, donor race, the time since fingerprint deposition, etc. Hence, it is of vital importance to provide related research below.

The value of the level 3 feature in sex determination has been evaluated in several studies. Nagesh et al. examined included the fingerprint samples of 230 Indians and reported there was no significant difference in the sweat pore sizes and frequency between both the males and females.[96] To be specific, the pore frequency of females and males were 8.40 and 8.83 pores/cm ridge, respectively. The pore sizes of males ranged from 69 μm to 284 μm and those of females were 66–287 μm. Preethi et al. found pore number less than or equal to 32 pores/cm$^2$ was more likely to be of male origin, whereas

more than or equal to 36 pores/cm$^2$ was more likely to be of female origin. No significant difference was detected in pore types and shapes.[97] Kumar and his co-workers conducted a study to observe the pore shapes of left thumb ink impressions.[98] They found the pore number was 2–4 pores/cm ridge, which demonstrated no difference in both males and females. However, circular or round pores possessed higher occurrence in males than females. Wang et al. detected the shift of pore location that the maximum longitudinal and transverse location shifts of males were 166.46 μm and 61.00 μm while those of the females were 73.08 μm and 45.88 μm.[99] Additionally, another study undertaken by the same group also indicated the pore sizes of males were larger than those of females.[27] Murlidharf concluded that ridge shapes had a certain advantage over the poroscopy in sex determination. The reason
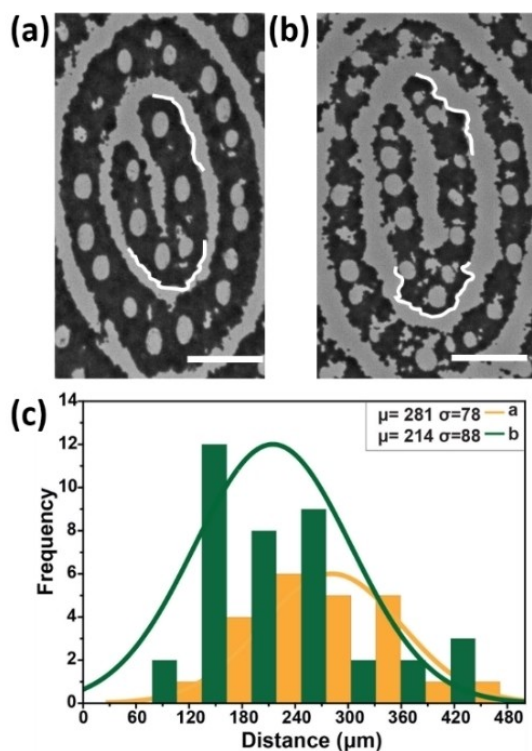
**Figure 13.** (a, b) Segments of two different fingerprints. (c) Frequency distribution of the distance between two adjacent sweat pores distributed along the ridge in a and b. Scale bars: 200 μm. Reproduced from Ref. [30] with permission of the Royal Society of Chemistry.

may be because the sample number of males whose 1 cm ridge had one concave edge was higher than that of females.[100]

Level 3 details were found useful in age determination. Nagesh et al. found pore size gradually increased, and the pore position and pore shape varied with the age.[96]

Level 3 features also have a relation to group differentiation. Singh et al. studied fingerprints deposited from Brahmins and Rajputs of Himachal Pradesh. They finally concluded that the pore size was different in both communities while no significant difference in pore frequency, interspacing, size, shape, and position.[101] Very recently, in the work of Govindarajulu et al., the ridge width of eleven criminals was found to vary in right and left hands while no significant differences were detected in normal people.[102]

It has been observed that ridge topography may change with latent fingerprints age advanced.[103] It has been reported by Preda and his co-workers that the ridge suffered narrowing and a loss in ridge continuity over time.[104]

### 4.3. Other applications

In addition to the above applications, level 3 features were applied to ascertain if a fingerprint is a forgery. Champod et al. proved the presence or absence of pores could be reasonably used in discriminating genuine from spoof transactions.[105] Additionally, several studies have indicated that the pore characteristics are

associated with some sweating-related medical diseases and thus have the potential to early diagnose such diseases.[106–107]

## 5. Summary and Future Prospects

Fingerprints carry sufficient and reliable discriminative characteristics which ensure their status in individualization. Over the past years, advances in analytical instruments and new technologies have accelerated the development of forensic chemistry, especially in level 3 characteristic detection and analysis. The visualization and application of level 3 features prove that the third-level features give additional information (gender, age, race, health, etc.) about the donor than just individualization.

In this review, four main sections are organized. The first part provides a brief introduction of the level 3 feature types along with the assessment of their quality and reliability. The second section summarizes the related techniques for detecting third-level features such as physical interaction methods, residue-responsive reagents, MS methods and electrochemical techniques. The third part highlights the application of level 3 characteristics, especially in personal identification, donor profiling (age, sex, race, etc.), fingerprint age determination, spoof fingerprint discrimination and even the diagnosis of sweat-related disease.

Although considerable state-of-the-art achievements have been attained in the third-level related field, the third-level details are rarely utilized during the fingerprint identification process.[14] The reasons are listed below: (i) The current visualization reagents for LFPs or deposition methods cannot well display the third-level structures.[15] For example, the powder reagent is frequently used for latent fingermark visualization relying on the electrostatic adsorption between the powder and fingerprint residues. Unfortunately, the powder easily aggregates and inevitably adheres to certain pore regions, resulting in the distortion of some microscopic details as well. Additionally, the traditional ink deposition method will contaminate fingertips and more importantly, excess ink will cover the level 3 features. (ii) Usually, the fingermarks are left at crime scenes with poor quality, whose level 3 features are insufficient or not well-reflected and thus can't be extracted for the following identification procedure. (iii) Besides, fingerprint images in fingerprint databases are routinely captured at the resolution of 500 ppi which cannot meet the standards of third-level feature extraction. In such a situation, the comparison can not be achieved even if the fingermarks at crime scenes possess enough level 3 features. (iv) Last but not least, no systematic and mature analytical methods have been developed for level 3 features. Although the emerging high-resolution ($\geq$ 1000 ppi) fingerprint imaging techniques have facilitated the growth of third-level-feature based algorithms, it is still a long way to go for improving the comparison accuracy. For instance, the pore alignment accuracy and only local feature extraction heavily affect the comparison result of pore-based algorithms.

Hence, several challenging issues need to be resolved before the implementation of level 3 features. Specifically, (i) developing reliable visualization methods that allow effective

**ChemistryOpen**

Review
doi.org/10.1002/open.202200091

Chemistry
Europe
European Chemical
Societies Publishing

extraction of level 3 features. First, as PVA-based or PDA-based papers exhibited exceptional performance in sweat pore mapping, whether they can be an alternative to forensic tape should be clarified in the future work. Second, some novel detection techniques such as MS imaging and SECM techniques show outperformance in level 3 feature detection, nevertheless, their long scanning time might hinder the implementation in forensic investigation practice. Hence, it is urgent to develop time-saving imaging strategies such as changing the scanning path into the zigzag or spiral mode to enable large-area imaging. Additionally, novel tips such as soft probes should be explored for using SECM to scan delicate samples with topographic sample features. Third, the compatibility of mentioned detection techniques with DNA analysis should constitute the further development steps to be investigated. (ii) Utilizing high-resolution fingerprint imaging or capture techniques in fingerprint database construction. Only in this way, can level 3 features of fingerprint samples in the database be extracted and compared with the fingermarks at crime scenes. (iii) Exploring multi parameters for the third level detail analysis and improving the accuracy of level-3-feature-based algorithms. The concept of level 3 details is often limited to the sweat pores which easily leads to information missing, whereas it can be broadened to ridge counters, such as the angle of bifurcations. We believe the application scenario can be expanded as more level 3 parameters are systematically investigated. (iv) Establishing standard measurement methods. Current research adopted various measurement methods of level 3 parameters. Under such circumstances, the comparison among different studies cannot be achieved. Hence, it is urgent to find out a scientific measurement method and unify it in future work. (v) As many fingerprint samples as possible should be investigated to screen out the characteristic parameters and verify the accuracy of prediction results as well. (vi) Focusing not only on level 3 details but other fingerprint information. Since the analysis methods of the third level details are still evolving and many mentioned techniques provide the chemical information of residues more than just physical image patterns, more parameters involving fingerprint patterns, minutiae and chemical components should be simultaneously considered and combined with level 3 features to support more robust individualization, donor profiling, spoof fingerprint differentiation, etc.

## Acknowledgements

## Conflict of Interest

The authors declare no conflict of interest.

## Data Availability Statement

The data that support the findings of this study are available from the corresponding author upon reasonable request.

[1] B. Su, *Anal. Bioanal. Chem.* **2016**, *408*, 2781–2791.
[2] H. S. Jung, J. Cho, K. C. Neuman, *Anal. Chim. Acta* **2021**, *1181*, 338850.
[3] M. Shi, Q. Wei, L. Tian, X. Du, X. Zhang, M. Zhang, *Electrochim. Acta* **2020**, *350*, 136373.
[4] H. Chen, M. Shi, R. Ma, M. Zhang, *Analyst* **2021**, *146*, 33–47.
[5] B. T. B. Wijerathne, *Anuradhapura Med. J.* **2015**, *9*, 44–46.
[6] C. Suresh, G. P. Darshan, S. C. Sharma M Venkataravanappa, H. B. Premkumar, S. Shanth, K. N. Venkatachalaiah, H. Nagabhushana, *Opt Mater* **2020**, *100*, 109625.
[7] Y. Li, C. Xu, C. Shu, X. Hou, P. Wu Chin, *Chem. Lett.* **2017**, *28*, 1961–1964.
[8] N. Singla, M. Kaur, S. Sofat, *Multimedia Tools Appl.* **2022**, 1–18.
[9] C. W. Schultz, J. X. H. Wong, H. Z. Yu, *Sci. Rep.* **2018**, *8*, 1–9.
[10] V. Soum, S. Park, A. I. Brilian, Y. Kim, M. Y. Ryu, T. Brazell, F. J. Burpo, K. K. Parker, O. Kwon, K. Shin, *ACS Omega* **2019**, *4*, 8626–8631.
[11] C. W. Schultz, M. Fawzy, F. Nasirpouri, K. L. Kavanagh, H. Yu ACS Appl, *Electron. Mater.* **2021**, *3*, 2097–2105.
[12] E. Locard, *Biol. Revue Sci. Med.* **1912**, *2*, 357–365.
[13] Y. Xu, G. Lu, Y. Lu, D. Zhang, *Pattern Recognit. Lett.* **2019**, *125*, 773–779.
[14] H. Khmila, S. Barhoumi, I. K. Kallel, N. Smaoui, H. Derbel, *In Advanced Methods for Human Biometrics*, Springer, Cham, Switzerland **2021**.
[15] A. Jain, Y. Chen, M. Demirkus, *in 18th Int. Conf. on Pattern Recognit., IEEE* **2006**, *4*, 477–480.
[16] A. Gupta, K. Buckley, R. Sutton, *Forensic Sci. Int.* **2008**, *179*, 172–175.
[17] K. Zhong, S. Lu, W. Guo, J. Su, S. Sun, J. Hai, B. Wang, *Chem. Commun.* **2021**, *57*, 9434–9437.
[18] A. Gupta, R. Sutton, *J. Forensic Sci.* **2010**, *55*, 970–975.
[19] A. Anthonioz, N. Egli, C. Champod, C. Neumann, R. Puch-Solis, A. Bromage-Griffiths, *J. Forensic Identif.* **2008**, *58*, 562–589.
[20] C. Champod, Supplementary report to the Fingerprint inquiry. Lausnne: Universite de Lausanne, Institut de police scientifique **2009**.
[21] S. B. Guo, S. W. Wang, Y. Wang, X. F. Fu, *Chin. J. Forensic Sci.* **2013**, *1*, 56–61. (in Chinese).
[22] Y. M. Wang, *Sci. Technol.* **2018**, *24*, 7–14. (in Chinese).
[23] D. R. Ashbaugh, *Fingerprint Whorld* **1982**, *8*, 36–38.
[24] A. R. Roddy, J. D. Stosz, *Proc. IEEE* **1997**, *85*, 1390–1421.
[25] A. Gupta, K. A. Buckley, R. Sutton, *Fingerprint Whorld* **2007**, *33*, 156–163.
[26] S. Oklevski, *Fingerprint Whorld* **2011**, *37*, 170–181.
[27] L. Liang, Y. M. Wang, J. M. Cao, *Forensic Sci. Technol.* **2022**, *47*, 246–251. (in Chinese).
[28] J. Kaur, M. Dhall, *Egypt. J. Forensic Sci.* **2022**, *12*, 1–9.
[29] Q. Zuo, Y. Zhou, *Chin. J. Forensic Sci.* **2020**, *113*, 55–59. (in Chinese).
[30] M. Shi, L. Zhao, H. Chen, L. Tian, R. Ma, X. Zhang, M. Zhang, *Anal. Methods* **2021**, *13*, 5564–5572.
[31] B. K. Sharma, R. Bashir, M. Hachem, H. Gupta Egypt, *J. Forensic Sci.* **2019**, *9*, 1–6.
[32] H. Li, Y. P. Luo, *Forensic Sci. Technol.* **2014**, 37–38. (in Chinese).
[33] K. L. Monson, M. A. Roberts, K. B. Knorr, S. Alia, S. B. Meagher, K. Biggs, P. Blumed, D. Brandellie, A. Marzioli, R. Reneau, F. Tarasih, *Forensic Sci. Int.* **2019**, *297*, 111–131.
[34] S. Oklevski, O. P. Jasuca, G. Singh, *Turk. J. Forensic Sci. Crime Stud.* **2019**, *1*, 36–49.
[35] Y. M. Wang, J. M. Cao, N. Liang, J. Y. Liu, X. H. Xie, Y. L. Li, *Forensic Sci. Technol.* **2020**, *45*, 480–485. (in Chinese).
[36] D. R. Ashbaugh, *Quantitative-qualitative friction ridge analysis: an introduction to basic and advanced ridgeology*, CRC press, Boca Raton, FL **1999**.
[37] A. R. Roddy, J. D. Stosz, *Intelligent biometric techniques in fingerprint and face recognition*, Routledge, London, UK **1999**.
[38] D. R. Ashbaugh, *J. Forensc Identif.* **1992**, *42*, 106–115.
[39] M. Stücker, M. Geil, S. Kyeck, K. Hoffman, A. Röchling, U. Memmel, P. Altmeyer, *J. Forensic Sci.* **2011**, *46*, 857–861.

**ChemistryOpen**

Review
doi.org/10.1002/open.202200091

**Chemistry Europe**
European Chemical
Societies Publishing

[40] L. R. V. Silva, L. L. Mizokami, P. R. Vieira, S. A. S. Kuckelhaus, *Forensic Sci. Int.* **2016**, *259*, 41–46.

[41] H. Wilder, B. Wentworth, *Personal Identification*, The Gorham Press, Boston, USA **1918**.

[42] T. Joshi, C. Mamat, H. Stephan, *ChemistryOpen* **2020**, *9*, 703–712.

[43] S. Shetty, N. Baig, M. Safa, R. Gharbi, S. Sriram, F. Rasoul, B. Alameddine, *ChemistryOpen* **2021**, *10*, 1067–1073.

[44] A. Gulino, G. Papanikolaou, P. Lanzafame, A. Aaliti, P. Primerano, L. Spitaleri, C. Triolo, Z. Dahrouch, A. Khaskhoussi, S. L. Schiavo, *ChemistryOpen* **2021**, *10*, 1033–1040.

[45] P. Wu, C. Xu, X. Hou, H. Y. Chen, *Chem. Sci.* **2015**, *6*, 4445–4450.

[46] A. Becue, S. Moret, C. Champod, P. Margot, *Forensic Sci. Int.* **2009**, *191*, 36–41.

[47] D. Navami, R. B. Basavaraj, G. P. Darshan, H. K. Inamdar, S. C. Sharma, H. B. Premkumar, H. Nagabhushana, *Opt. Mater.* **2019**, *88*, 479–487.

[48] C. Suresh, G. P. Darshan, S. C. Sharma, M. Venkataravanappa, H. B. Premkumar S Shanthi, K. N. Venkatachalaia, H. Nagabhushana, *Opt. Mater.* **2020**, 100, 109625.

[49] H. Singh, R. Sharma, G. Bhargava, S. Kumar, P. Singh New, *J. Chem.* **2018**, *42*, 12900–12907.

[50] R. Suresh, S. K. Thiyagarajan, P. Ramamurthy, *Sens Actuators* **2018**, *258*, 184–192.

[51] Y. L. Wang, C. Li, H. Q. Qu, C. Fan, P. J. Zhao, R. Tian, M. Q. Zhu J Am, *Chem. Soc.* **2020**, *142*, 7497–7505.

[52] Q. Wei, X. Li, X. Du, X. Zhang, M. Zhang, *Sci. China Chem.* **2017**, *60*, 1250–1257.

[53] P. Feng, N. Pan, B. Song, *Compos. Commun.* **2020**, *22*, 100479.

[54] Y. Wang, J. Wang, Q. Ma, Z. Li, Q. Yuan, *Nano Res.* **2018**, *11*, 5499–5518.

[55] S. Yang, C. F. Wang, S. Chen, *Angew. Chem. Int. Ed.* **2011**, *50*, 3706–3709; *Angew. Chem.* **2011**, *123*, 3790–3793.

[56] J. Lee, M. Pyo, S. Lee, J. Kim, M. Ra, W. Y. Kim, B. J. Park, C. W. Lee, J. M. Kim, *Nat. Commun.* **2014**, *5*, 1–10.

[57] C. W. Lee, B. J. Park M Pyo, J. Lee, W. Baek, C. W. Lee, B. J. Park, J. M. Kim, *Chem. Commun.* **2015**, *51*, 3177–3180.

[58] D. H. Park, W. Jeong, M. Seo, B. J. Park, J. M. Kim, *Adv. Funct. Mater.* **2016**, *26*, 498–506.

[59] M. Seo, D. H. Park, B. J. Park, J. M. Kim, *J. Appl. Polym. Sci.* **2017**, *134*, 44419.

[60] Q. Lou, S. Qu, P. Jing, W. Ji, D. Li, J. Cao, H. Zhang, L. Liu, J. Zhao, D. Shen, *Adv. Mater.* **2015**, *27*, 1389–1394.

[61] P. Zhang, Z. An, J. He, W. Sheng, L. Wang, L. Tao, B. Zhou, *J. Lumin.* **2022**, *244*, 118735.

[62] S. Cadd, M. Islam, P. Manson, S. Bleay, *Sci. Justice* **2014**, 55, 219–238.

[63] R. S. Li, J. H. Liu, T. Yang, P. F. Gao, J. Wang, H. Liu, S. J. Zhen, Y. F. Li, C. Z. Huang, *Anal. Chem.* **2019**, *91*, 11185–11191.

[64] R. S. Ramotowski, *Composition of latent print residue*. CRC Press, Boca Raton, USA **2001**.

[65] V. Drapel, A. Becue, C. Champod, P. Margot, *Forensic Sci. Int.* **2009**, *184*, 47–53.

[66] A. Dam, M. C. G. Aalders, T. G. Leeuwen, S. A. G. Lambrechts, *J. Forensic Sci.* **2013**, *58*, 999–1002.

[67] A. Dam, M. C. G. Aalders, M. Puit, S. M. Gorré, D. Irmaka, T. G. Leeuwen, S. A. G. Lambrechts, *Sci Justice* **2014**, *54*, 356–362.

[68] A. Dam, K. A. Nes, M. C. G. Aalders, T. G. Leeuwen, S. A. G. Lambrechts, *Anal Methods* **2014**, *6*, 1051–1058.

[69] Y. He, L. Xu, Y. Zhu, Q. Wei, M. Zhang, B. Su, *Angew. Chem. Int. Ed.* **2014**, *53*, 12609–12612; *Angew. Chem.* **2014**, *126*, 12817–12820.

[70] L. Xu, Z. Cao, R. Ma, Z. Wang, Q. Qin, E. Liu, B. Su Anal, *Chemistry* **2019**, *91*, 12859–12865.

[71] N. Achetib, A. Weert, M. Birkl, T. G. Leeuwen, M. C. G. Aalders, A. Dama, *Forensic Sci. Int.: Genet.* **2021**, *52*, 102485.

[72] A. Dam, M. C. G. Aalders, K. Braak, H. J. J. Hardy, T. G. Leeuwen, S. A. G. Lambrechts, *Forensic Sci. Int.* **2013**, *232*, 173–179.

[73] A. Dam, K. Falkena, S. A. Daas, I. Veldhuizen, M. C. G. Aalders, *Forensic Sci. Int.* **2021**, *324*, 110804.

[74] J. Zhao, K. Zhang, Y. Li, J. Ji, B. Liu, *ACS Appl. Mater. Interfaces* **2016**, *8*, 14389–14395.

[75] C. Elsner, B. Abel, *Sci. Rep.* **2014**, *4*, 1–6.

[76] T. M. Guinan, O. J. R. Gustafsson, G. McPhee, H. Kobus, N. H. Voelcker, *Anal. Chem.* **2015**, *87*, 11195–11202.

[77] M. J. Bailey, M. Ismail, S. Bleay, N. Bright, M. L. Elad, Y. Cohen, B. Geller, D. Everson, C. Costa, R. P. Webb, J. F. Watts, M. Puit, *Analyst* **2013**, *138*, 6246–6250.

[78] L. Cai, M. C. Xia, Z. Wang, Y. B. Zhao, Z. Li, S. Zhang, X. Zhang, *Anal. Chem.* **2017**, *89*, 8372–8376.

[79] T. D. Thandauthapani, A. J. Reeve, A. S. Long, I. J. Turner, J. S. Sharp, *Sci. Justice* **2018**, *58*, 405–414.

[80] W. J. Li, L. H. Sun, W. You, L. X. Wang, Y. B. Zhao, Z. P. Li, *Chin. J. Anal. Chem.* **2020**, *48*, 1511–1518.

[81] C. Yuan, M. Li, M. Wang, H. Cao, T. Lin, *Electrochim. Acta* **2021**, *390*, 138798.

[82] L. Xu, Y. Li, S. Wu, X. Liu, B. Su, *Angew. Chem. Int. Ed.* **2012**, *124*, 8192–8196.

[83] Y. Li, L. Xu, Y. He, B. Su, *Electrochem. Commun.* **2013**, *33*, 92–95.

[84] M. Carano, N. Lion, J. P. Abid, H. H. Girault, *Electrochem. Commun.* **2004**, *6*, 1217–1221.

[85] M. Zhang, H. H. Girault, *Electrochem. Commun.* **2007**, *9*, 1778–1782.

[86] N. Singla, M. Kaur, S. Sofat, *Forensic Sci. Int.* **2020**, *309*, 110187.

[87] D. Agarwal, A. Bansal, *Multimedia Tools Appl.* **2021**, *80*, 23605–23624.

[88] Z. Shen, Y. Xu, G. Lu, *2019 IEEE Symp. Ser. Comput. Intell. IEEE* **2019**, 426–432.

[89] Z. Shen, Y. Xu, J. Li, G. Lu, *IEEE Int. Conf. Image Process. IEEE* **2019**, 2581–2585.

[90] V. L. Jothi, S. Arumugam, *Int. J. Comput. Appl.* **2012**, *48*, 19–22.

[91] D. Jorgenson, *Fingerprint Whorld* **1998**, *24*, 102–105.

[92] R. D. Reneau, *J. Forensic Identif.* **2003**, *53*, 531–537.

[93] J. Zhou, F. Chen, N. Wu, C. Wu, *Pattern Recognit.* **2009**, *42*, 896–906.

[94] Q. Zhao, J. Feng, A. K. Jain, *MSU Tech. Rep.* **2010**, *8*, 1–30.

[95] M. P. Segundo, R. Paula Lemes, *Proc. IEEE Conf. Comput. Vis. Pattern Recognit. Workshops* **2015**, 128–133.

[96] K. R. Nagesh, S. Bathwal, B. Ashoka, *J. Forensic Leg. Med.* **2011**, *18*, 302–305.

[97] D. S. Preethi, M. D. Nithin, B. Manjunatha, B. M. Balaraj, *J. Forensic Sci.* **2012**, *57*, 449–452.

[98] V. Bhagwat, D. M. Kumar, K. Naga, *Sch. Int. J. Anat. Physiol.* **2020**, *3*, 53–56.

[99] Y. M. Wang, J. M. Cao, N. Liang, J. Y. Liu, X. H. Xie, Y. L. Li, *Forensic Sci. Technol.* **2020**, *45*, 480–485. (in Chinese).

[100] M. Dhoot, G. V. Murlidhar, *Int. J. Sci. Res.* **2019**, *8*, 17–18.

[101] R. K. Singh, M. P. Sachdeva, *Ind. J. Phys. Anthrop. Hum. Genet.* **2013**, *32*, 343–371.

[102] R. B. Govindarajulu, S. Saha, M. Parmar, *Int. J. New Innovations Eng. Technol.* **2020**, *13*, 41–44.

[103] J. De Alcaraz-Fossoul, C. Barrot-Feixat, S. C. Zapico, M. Mancenido, J. Broatch, K. A. Roberts, C. Carreras-Marin, J. Tasker, *J. Forensic Sci.* **2018**, *63*, 1085–1091.

[104] G. Popa, R. Potorac, N. Preda, *Rom. J. Legal Med.* **2010**, *18*, 149–154.

[105] M. Espinoza, C. Champod, *2011 Int.Conf. Hand-Based Biom. IEEE* **2011**, 1–5.

[106] D. H. Park, B. J. Park, J. M. Kim Acc, *Chem. Res.* **2016**, *49*, 1211–1222.

[107] D. Berg, D. H. Weingold, K. G. Abson, *Arch. Dermatol.* **1990**, *126*, 1075–1079.